Research Paper

Electrophilic nitro-fatty acids suppress psoriasiform dermatitis: STAT3 inhibition as a contributory mechanism

Peng Wang [a], Meaghan E. Killeen [a], Tina L. Sumpter [a,b], Laura K. Ferris [a], Louis D. Falo Jr. [a,d], Bruce A. Freeman [c], Francisco J. Schopfer [c,e,f], Alicia R. Mathers [a,b,*]

[a] Departments of Dermatology, University of Pittsburgh School of Medicine. Pittsburgh, PA 15261, USA
[b] Immunology, University of Pittsburgh School of Medicine. Pittsburgh, PA 15261, USA
[c] Pharmacology and Chemical Biology, University of Pittsburgh School of Medicine. Pittsburgh, PA 15261, USA
[d] Bioengineering, University of Pittsburgh School of Medicine. Pittsburgh, PA 15261, USA
[e] Pittsburgh Heart, Lung and Blood Vascular Medicine Institute, University of Pittsburgh School of Medicine. Pittsburgh, PA 15261, USA
[f] Pittsburgh Liver Research Center, University of Pittsburgh School of Medicine. Pittsburgh, PA 15261, USA

ABSTRACT

Psoriasis is a chronic inflammatory skin disease with no cure. Although the origin of psoriasis and its underlying pathophysiology remain incompletely understood, inflammation is a central mediator of disease progression. In this regard, electrophilic nitro-fatty acids (NO_2–FAs) exert potent anti-inflammatory effects in several *in vivo* murine models of inflammatory diseases, such as chronic kidney disease and cardiovascular disease. To examine the therapeutic potential of NO_2–FAs on psoriasiform dermatitis, we employed multiple murine models of psoriasis. Our studies demonstrate that oral treatment with nitro oleic acid (OA-NO_2) has both preventative and therapeutic effects on psoriasiform inflammation. In line with this finding, oral OA-NO_2 downregulated the production of inflammatory cytokines in the skin. *In vitro* experiments demonstrate that OA-NO_2 decreased both basal IL-6 levels and IL-17A-induced expression of IL-6 in human dermal fibroblasts through the inhibition of NF-κB phosphorylation. Importantly, OA-NO_2 diminished STAT3 phosphorylation and nuclear translocation via nitroalkylation of STAT3, which inhibited keratinocyte proliferation. Overall, our results affirm the critical role of both NF-κB and STAT3 in the incitement of psoriasiform dermatitis and highlight the pharmacologic potential of small molecule nitroalkenes for the treatment of cutaneous inflammatory diseases, such as psoriasis.

1. Introduction

Psoriasis is a chronic inflammatory skin disease affecting 2–3% of the US population. It is characterized by an infiltration of cutaneous inflammatory cells releasing cytokines, growth factors, and chemokines that modulate keratinocyte differentiation and proliferation [1]. Our understanding of the pathophysiology of psoriasis has significantly progressed in the past decade. In this regard, advancement in our molecular knowledge has led to an improved understanding of psoriasis; thus, influencing the development of efficient therapeutics, including TNF-α inhibitors and IL-17A antibodies [2]. Although new biologics have improved therapeutic options, in general, patients need lifelong therapies and current therapies predominantly rely on systemic acting immuno-suppressive drugs, for which long-term adverse effects, significant costs, morbidity, sex differences, and loss of effectiveness remain a concern [3–5]. Therefore, the development of an oral therapeutic agent that reversibly and specifically inhibits signaling pathways and inflammation in psoriasis pathogenesis is paramount.

Naturally occurring electrophilic nitro-fatty acids (NO_2–FAs) are nitration products of unsaturated fatty acids that mediate anti-inflammatory, antioxidant, and cytoprotective actions [6,7]. The therapeutic potential of NO_2–FAs has been demonstrated in several *in vivo* murine models of inflammatory diseases, such as chronic kidney disease, cardiovascular disease, diabetes, and allergic contact dermatitis [8–12]. The primary mechanism whereby NO_2-FA regulate metabolic, cell signaling, and anti-inflammatory responses is via nitroalkylation, a

post-translational protein modification representing the adduction of nucleophilic amino acids such as cysteine and histidine by the electrophilic β-carbon of the nitroalkene substituent [13]. In this regard, nitro oleic acid ($OA-NO_2$), a prototypical NO_2-FA, displays an anti-inflammatory role in preventing and treating various model system disease phenotypes by modulating redox-sensitive transcription factors, receptors, and proteins including PPARγ, NF-κB, Keap1/Nrf2, STING and heat-shock factor response [6,14,15]. CXA-10, the specific $10-NO_2$-OA isomer, is currently in Phase II clinical trials aimed at treating vascular and pulmonary diseases.

Our previous study demonstrated that subcutaneous injections of $OA-NO_2$ inhibit and treat contact hypersensitivity (CHS) in a murine model [8]. However, the therapeutic effect of $OA-NO_2$ on psoriasis is still unknown. Importantly, $[^{14}C]10-NO_2$-OA and LC-MSMS studies have revealed that >95% of systemically-absorbed $10-NO_2$-OA is esterified in chylomicron triglycerides [16]. This distribution mechanism's main pharmacokinetic consequences are a) the limitation of nitroalkene inactivation during absorption and circulation and b) avoidance of hepatic first pass degradation, thus facilitating free fatty acid nitroalkene delivery to tissues upon the hydrolysis of triglycerides containing esterified nitroalkene fatty acids by capillary lipoprotein lipases. This fatty acid acquisition mechanism is also actively used by the skin to sustain ceramide, sphingolipid, and triglyceride synthesis, with the skin being the tissue most affected by deficits in essential fatty acids. The present study tested the hypothesis that small molecule nitroalkenes such as NO_2-FA display anti-psoriatic actions by regulating redox-sensitive transcription factors central to the development of psoriasis, including NF-κB and STAT3.
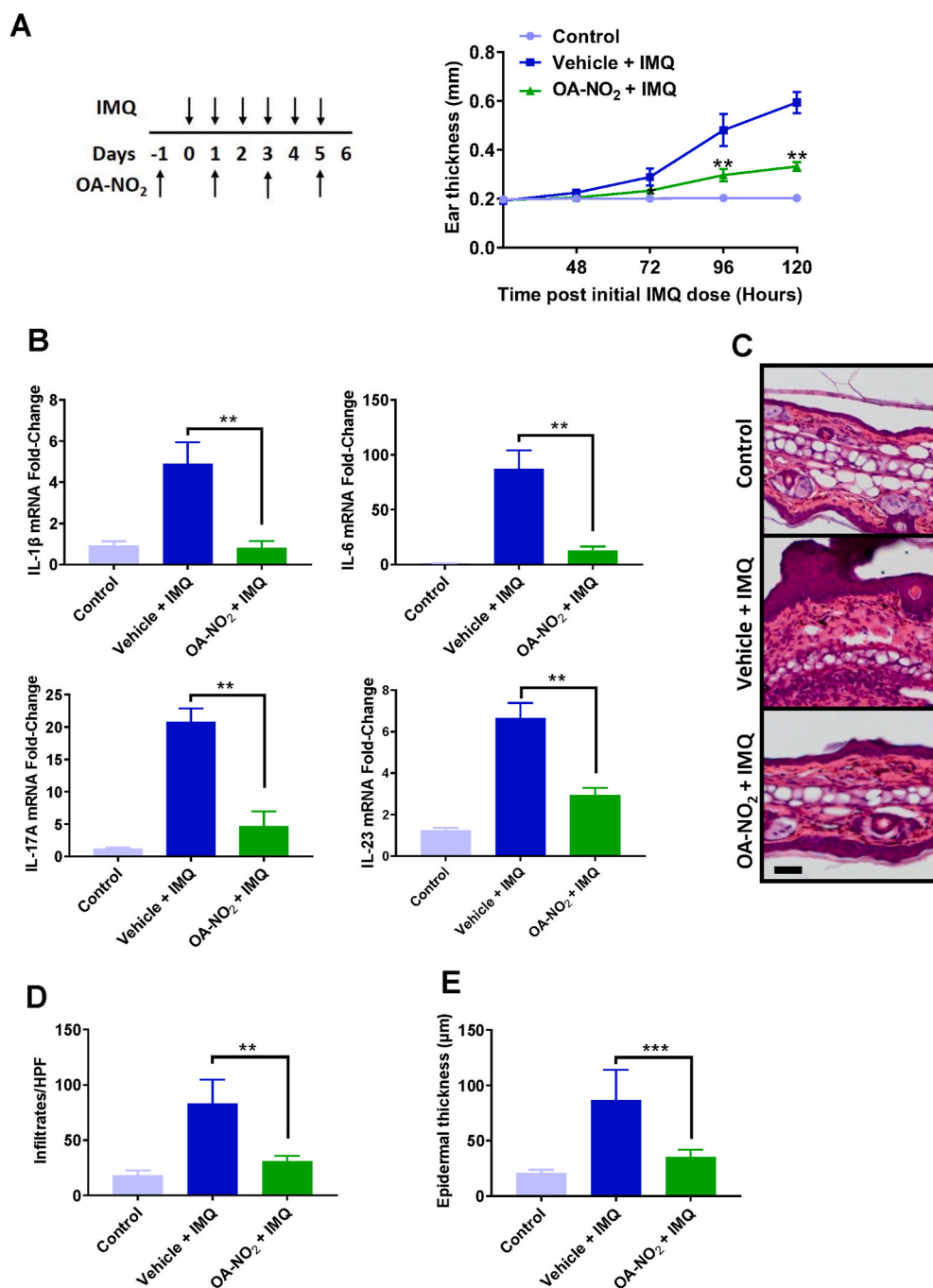
Fig. 1. Oral $OA-NO_2$ inhibits IMQ-induced psoriasis-like skin inflammation. (A) C57BL/6 mice were treated with $OA-NO_2$ or vehicle control orally and IMQ topically, according to the schematic. Ear thickness was measured following IMQ administration. Each point represents the mean ± SEM from 5 mice per group. Data are one representative of three independent experiments. *$p < 0.05$, **$p < 0.01$. (B) IL-1β, IL-6, IL-23, and IL-17A mRNA levels in ear tissue were examined 48 h following IMQ treatment. Bars represent the mean ± SEM from 3 to 5 mice per group with each sample ran in triplicates, **$p < 0.01$. (C) Six d following IMQ treatment ears were excised and cross-sections were stained with H&E. Scale bar = 50 μm. (D–E) Infiltrates (D) and Epidermal thickness (E) were quantitated. Bars represent the mean ± SEM from 4 to 5 mice per group, ten independent high powered field (HPF) measurements were averaged from each mouse, **$p < 0.01$ and ***$p < 0.001$.

2. Results and discussion

2.1. Protective effect of oral OA-NO2 on acute models of psoriasis

To test our hypothesis that OA-NO2 can inhibit psoriasiform inflammation, we evaluated two acute models of psoriasis (imiquimod; IMQ and rmIL-23), termed psoriasiform dermatitis, in C57BL/6 mice. These models share many features of human psoriasis, including pronounced cutaneous inflammation characterized by epidermal thickening (acanthosis), inflammatory cell infiltration, microabscess formation, and the increased production of inflammatory cytokines, including IL-1β, IL-6, IL-23, IL-17A, and TNF-α [17–20]. We first assessed the effect of oral OA-NO2 on the IMQ-induced psoriasiform model. For this, mice were administered oral OA-NO2 or vehicle control 18 h prior to topical IMQ application to dorsal skin and ears, according to Fig. 1A schematic. Ear thickness significantly decreased in OA–NO2–treated mice after 72 h, compared to IMQ treatments alone (Fig. 1A). Moreover, OA-NO2 also significantly suppressed transcripts of inflammatory cytokines characteristic of psoriasis including IL-1β, IL-6, IL-17A, and IL-23 (Fig. 1B). TNF-α expression decreased but did not reach statistical significance ($p = 0.06$; Fig. S1). Consistent with the protective role of OA-NO2 in skin inflammation, histological analysis demonstrated a significant decrease in inflammatory infiltrates and epidermal thickness in ear skin of mice treated with OA-NO2, compared to IMQ treatments alone (Fig. 1C, D, and E). Similar results were obtained when dorsal back skin was assessed (data not shown).

In a second set of experiments, the rmIL-23 psoriasiform model was induced according to the schematic in Fig. 2A. Oral OA-NO2 or vehicle control was administered 18 h prior to rmIL-23 ear injections and then every other d for 10 d. Similar to the IMQ model, OA-NO2 significantly blocked the increase in ear thickness induced following IL-23 injections

(Fig. 2A). Furthermore, OA-NO2 significantly suppressed IL-1β, IL-6, and IL-17A mRNA transcript levels compared to vehicle controls (Fig. 2B). Histological analysis of ear tissues demonstrated that OA-NO2 significantly inhibited cellular infiltration and epidermal thickening compared to rmIL-23 treatments alone (Fig. 2C–E). Together these data indicate that OA-NO2 has an inhibitory effect on the pathogenesis of acute psoriasiform skin inflammation.

2.2. Therapeutic and preventative properties of oral OA-NO2 on psoriasiform inflammation in chronic murine models

To assess whether OA-NO2 treatment has therapeutic and preventative effects on psoriasiform inflammation in chronic murine models, we utilized K14-VEGF transgenic mice. VEGF is highly expressed in psoriatic lesions and is a critical cytokine mediating angiogenesis [21, 22]. The ears and facial region of K14-VEGF mice gradually develop psoriatic-like features, including red and scaly plaques, epidermal thickening, parakeratosis, inflammatory infiltrate, and epidermal microabscesses [23] and (Fig. 3).

The therapeutic capacity of OA-NO2 was evaluated in 9 to 10-wk-old K14-VEGF mice with an ear thickness of 0.5 mm and the development of red scaly plaques on both ears. As diagramed in Fig. 3A, oral OA-NO2 or vehicle control was administrated every other day for 12 wk. Ear thickness was measured every wk for 5 wk; after this time point plaques on the ear interfered with measurements. The results demonstrate that OA-NO2 significantly suppressed ear thickness compared to vehicle control (Fig. 3B). The redness and plaque formation (scabbing) on the ears and face were likewise inhibited by OA-NO2 treatment, compared to vehicle controls (Fig. 3C and D). In line with the clinical and phenotypical findings, molecular analysis demonstrated a significant reduction in IL-1β, IL-6, and IL-17A transcripts, compared to vehicle
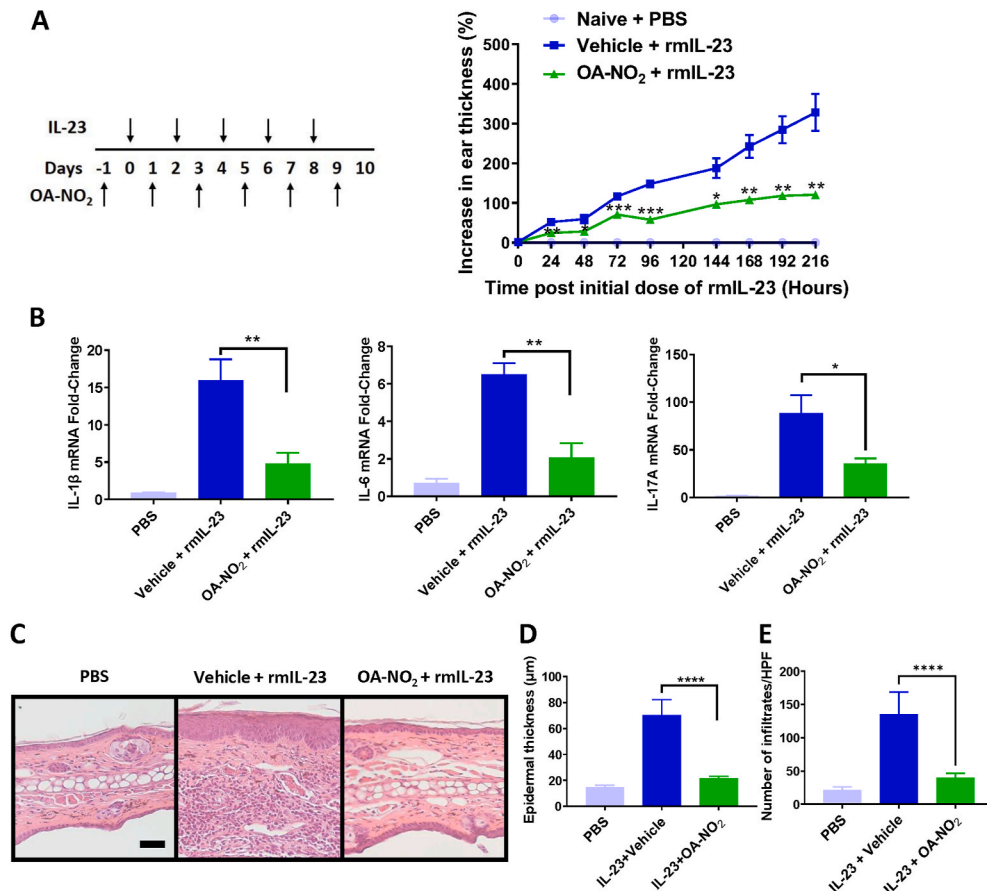
Fig. 2. Oral OA-NO2 inhibits IL-23-induced psoriasis-like skin inflammation. (A) OA-NO2 or vehicle control were orally administrated to C57BL/6 mice and rmIL-23 was injected subcutaneously into the ears, according to the schematic. The ear thickness was measured daily 24–216 h (120 h time-point was not acquired in this representative experiment) following rmIL-23 administration. Each point represents the mean ± SEM from 4 mice per group. Data are representative of three independent experiments. *indicates a significant difference compared with the vehicle control group at each time point, *$p < 0.05$, **$p < 0.01$, ***$p < 0.001$. (B) IL-1β, IL-6, and IL-17A mRNA levels were determined 240 h following rmIL-23 injection. Bars represent the mean ± SEM from 3 to 4 mice per group with each sample ran triplicates, *$p < 0.05$, **$p < 0.01$. Representative of two independent experiments. (C) Following 240 h of treatment ears were excised amd cross-sections were stained with H&E. Scale bar = 50 μm. (D) Epidermal thickness and (E) cellular infiltrate were quantitated. Bars represent the mean ± SEM from 4 mice per group, ten independent HPF measurements were averaged from each mouse, ****$p < 0.0001$.
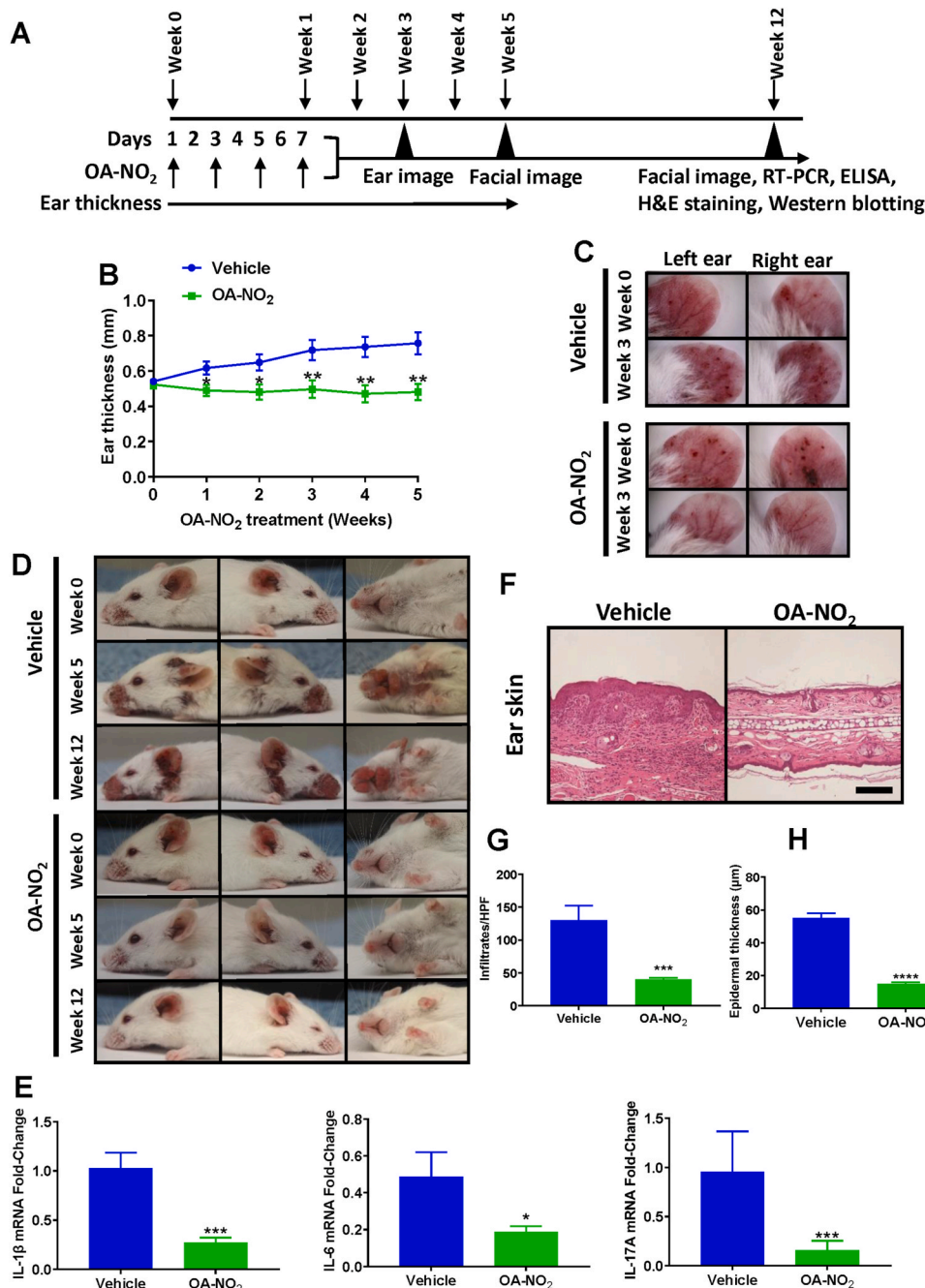
Fig. 3. Oral OA-NO₂ has a therapeutic effect on psoriasiform inflammation in the K14-VEGF mouse model. (A) OA-NO₂ or vehicle control was orally administrated to K14-VEGF mice according to schematic. (B) Ear thickness was measured weekly for five weeks and each point represents the mean ± SEM of 10 mice per group. Data are one representative of two independent experiments. *$p < 0.05$, **p ‹ 0.01. (C and D) Phenotypical presentation of mouse ears (C) and facial region (D) at indicated times. (E) IL-1β, IL-6, and IL-17A mRNA levels in ear tissues were determined following 12 wk of treatment. Bars represent the mean ± SEM from 6 mice per group with each sample ran triplicate, *$p < 0.05$, ***p ‹ 0.001. (F) Following 12 wk of treatments ears were excised and cross-sections were stained with H&E. Scale bar = 100 μm. (G–H) Infiltrates (G) and epidermal thickness (H) were quantitated. Bars represent the mean ± SEM from 5 mice per group, ten independent HPF measurements were averaged from each mouse, ***p ‹ 0.001 and ****p ‹ 0.0001.

controls (Fig. 3E). Histological analysis of ear cross-sections also exhibited a significant reduction of epidermal thickening and cellular infiltration in the OA–NO₂–treated group (Fig. 3F, G, and H).

To assess the capacity of OA-NO₂ to block the development of psoriasis-like lesions, we utilized 6 to 8-wk-old K14-VEGF mice that had minimal or no signs of inflammation, the ear thickness of these mice was less than 0.4 mm with no redness or only a pale tint of redness. Oral OA-NO₂ or vehicle control was administered every other day for 12 wk. Results in the preventative model mirrored those in the therapeutic model by preventing the development of lesions (Fig. S2).

To further confirm the therapeutic effect of OA-NO₂ on psoriasiform inflammation, we utilized an alternative K5-IL-17C model of psoriasis. By 8–10 weeks of age K5-IL-17C mice have developed red scaly plaques and significant hair loss, indicating a fully developed psoriasiform inflammatory response [24]. At this point, OA-NO₂ was administered

every other day for 2 wk following disease manifestation, including hair loss and lesional development on the dorsal neck and back (Fig. S3A). Within 2 wk, lesions had considerably progressed in the vehicle-treated group; however, following treatment with OA-NO₂ disease progression was halted (Fig. S3B). Additionally, IL-1β and IL-6 transcripts were significantly downregulated following OA-NO₂ treatment, compared to the vehicle controls (Fig. S3C). Histological examination of non-lesional and lesional skin from K5-IL-17C mice also confirmed that OA-NO₂ resolved established psoriasiform inflammation, as evidenced by a significant decrease in epidermal thickness and inflammatory infiltrate (Figs. S3D and S3E).

Overall, utilizing both acute and chronic murine models of psoriasis, we determined that OA-NO₂ has the capacity to improve the disease course and inhibit psoriasiform dermatitis, leading to the normalization of keratinocyte proliferation and cutaneous inflammation. In this

regard, OA-NO$_2$ suppressed the expression of critical inflammatory cytokines such as IL-1β, IL-6, and IL-17A.

2.3. Capacity of OA-NO$_2$ to inhibit STAT3 and NF-κB phosphorylation and IL-6 production in vivo

STAT3 is a cytoplasmic transcription factor that transmits signals to the nucleus following stimulation with psoriasis-associated cytokines, such as IL-6 [25]. Binding of IL-6 to its receptor induces activation of tyrosine-protein kinase JAK2, which mediates phosphorylation of STAT3 at Tyrosine 705 (Tyr705) [26]. Phosphorylation induces STAT3 nuclear translocation where it controls the expression of genes involved in cellular proliferation, differentiation, migration, survival, and oncogenesis [27]. Importantly, STAT3 phosphorylation is enhanced in lesional psoriatic skin along with increased cytokines and growth factors that stimulate STAT3 activation, such as IL-6 [28–31]. Moreover, STAT3 is involved in the psoriasis-dependent IL-23 signaling pathway [32]. Transgenic mice constitutively over-expressing STAT3 in keratinocytes develop cutaneous lesions reminiscent of human psoriatic lesions [30, 31]. Thus, STAT3 is a well-established potential drug target to treat psoriasis [31,33,34]. In M1 and M2 macrophages OA-NO$_2$ inhibits the

activation of STAT1, STAT3, and STAT6 when activated by LPS and IL-4 [35]. In order to determine whether OA-NO$_2$ manifests anti-psoriatic actions *in vivo* through modulation of STAT3, we assessed the outcome of OA-NO$_2$ on STAT3 phosphorylation in our murine models of psoriasis. Immunoblot analysis of ear homogenates demonstrated that OA-NO$_2$ was capable of significantly impairing STAT3 Tyr705 phosphorylation induced following IMQ treatment and in the chronic K14-VEGF model (Fig. 4A and B). However, there was not a significant decrease in pSTAT3 in the K5-IL-17c model (Fig. 4C). In line with previous findings [6,36], data confirm the capacity of OA-NO$_2$ to significantly inhibit phosphorylation of NF-κB p65 subunit in the K14-VEGF model (Fig. 4B). Whereas a significant suppression of NF-κB p65 phosphorylation was not detected in the IMQ and K5-IL-17c models (Fig. 4A and C). The lack of an inhibition of pSTAT3 in the K5-IL-17c model and pNF-κB in the IMQ and K5-IL-17c models is likely due to tissue collection timing, as these measurements were performed at the conclusion of the experiments and these transcription factors have a short window of activation. This supports an effect of OA-NO$_2$ that begins early in the inflammatory cycle. Moreover, it is expected that OA-NO$_2$ has additional as yet identified targets in these mouse models, beyond pSTAT3 and NF-κB. In this regard, the activation of the DNA sensing STING pathway is also
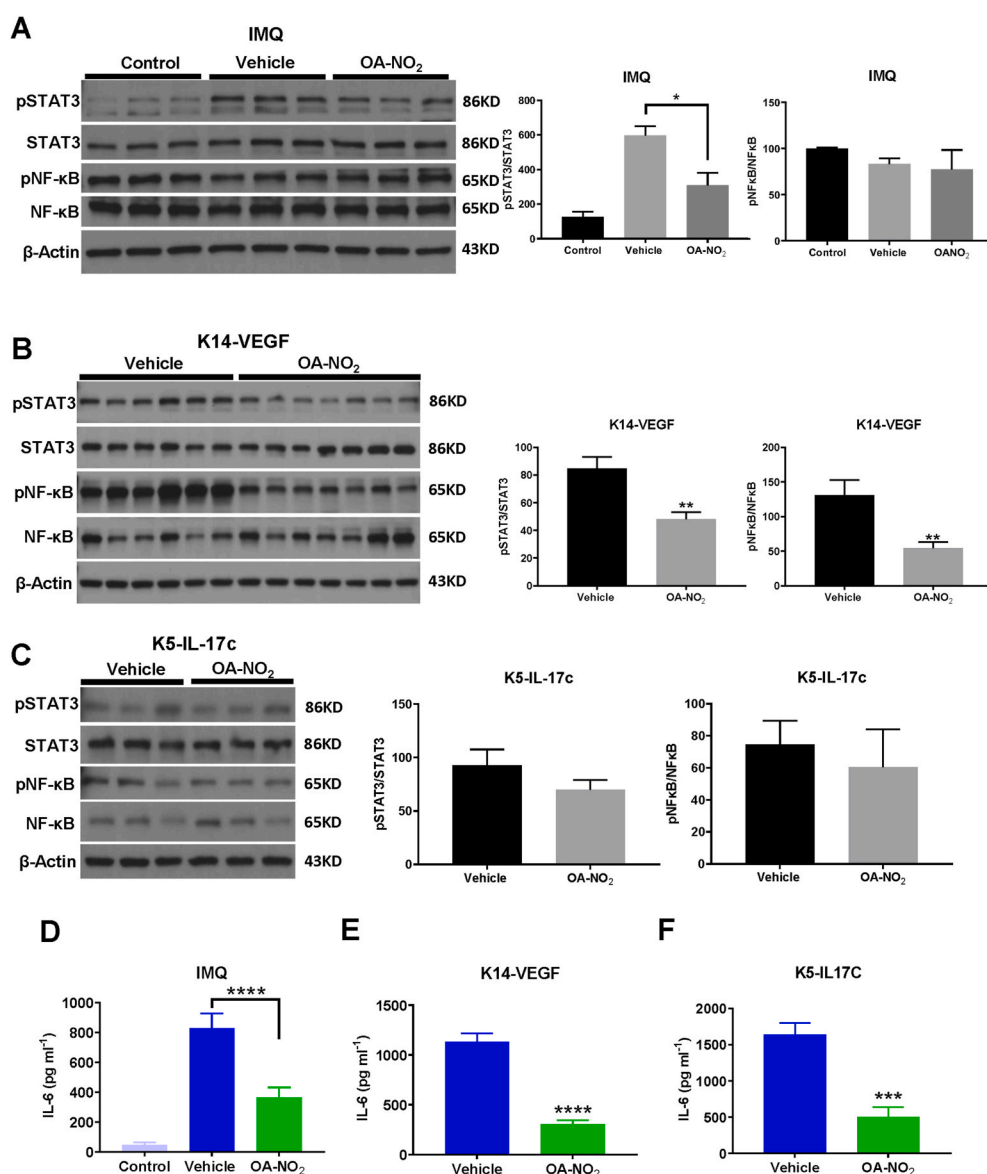
Fig. 4. OA-NO$_2$ inhibits STAT3 and NF-κB phosphorylation and reduces production of IL-6 *in vivo*. **(A–C)** STAT3, pSTAT3, NF-κB, and pNF-κB levels in cutaneous ear homogenates were determined by immunoblotting analysis. β-Actin levels were used as internal loading controls. Skin was harvested (A) 6 d following IMQ treatment in C57BL/6 mice, (B) after 12 wks of OA-NO$_2$ treatment in K14-VEGF mice, and (C) following 2 wk of OA-NO$_2$ treatment in K5-IL-17C mice, representative blots are presented. Densitometry results are plotted in the bar graphs (IMQ, n = 4–5: K14-VEGF, n = 12–13: K5-IL17c, n = 4). Phophorylated band intensities were quantified by ImageJ software and normalized to total STAT3 or NF-κB expression. (D–F) IL-6 protein levels were assessed in cutaneous homogenates by ELISA. Bars represent the mean ± SEM from 5 mice per group with each sample ran in triplicate. *$p < 0.05$, **$p < 0.01$, ***$p < 0.001$ and ****$p < 0.0001$.

targeted by nitro fatty acids [37]. These inflammatory pathways are represented differentially in the various psoriasis models and likely are inhibited by nitro fatty acids differentially, explaining why the observed decrease in epidermal thickness in the K5-IL-17c model (Fig. 3D) is not as pronounced as in the other psoriasis models.

IL-6 is one of the major cytokines mediating activation of STAT3 in the course of psoriatic lesional development [38]. Therefore, we further examined IL-6 protein expression in the skin. As shown in Fig. 4D–F, OA-NO$_2$ significantly inhibits production of IL-6 induced in both acute and chronic models. Together these *in vivo* data suggest that OA-NO$_2$ inhibits psoriasiform inflammation, in part, by blockade of IL-6 production and STAT3 phosphorylation.

2.4. OA-NO$_2$ suppresses NF-κB and STAT3 signaling in vitro

Multiple autoimmune inflammatory diseases are dependent on IL-6 and IL-17A [38]. In this regard, IL-6 is one of the main inducers of Th17 differentiation and function [32]. Data presented herein demonstrate that OA-NO$_2$ inhibits IL-6 expression in both acute and chronic psoriatic dermatitis. Previous studies indicate that fibroblasts have an IL-17A-initiated positive-feedback loop of IL-6 production, dependent on NF-κB signaling [38,39]. To evaluate whether OA-NO$_2$ exerts an anti-inflammatory effect via regulation of an IL-17A/IL-6 positive-feedback loop, we first analyzed the outcome of OA-NO$_2$ treatments on rhIL-17A-induced IL-6 expression in normal human dermal fibroblasts (NHDFs). OA-NO$_2$ treatment significantly decreased basal expression and rhIL-17A-induced expression of IL-6, compared to OA (corresponding native fatty acid control) and vehicle controls (Fig. 5A).

We further assessed the ability of OA-NO$_2$ to inhibit NF-κB signaling in our model system. Importantly, OA-NO$_2$ inhibits NF-κB signaling by multifaceted mechanisms [6,36,40]. The first-described and most prominent mechanism involves the nitroalkylation of the highly conserved Cys38 in the NF-κB p65 subunit. This nitroalkylation inhibits p65 phosphorylation and blocks NF-κB binding to the DNA Rel homology domain, which subsequently inhibits the transcription of inflammatory genes [6]. The second mechanism involves the inhibition of IKK-β, which prevents the degradation of the NF-κB IκBα inhibitory subunit. Under basal conditions, IκBα represses p65 and NF-κB activation. Additionally, p65 is regulated through polyubiquitination and proteasomal degradation [6,41]. Thus, we assessed the capacity of OA-NO$_2$ to suppress NF-κB signaling in fibroblasts treated with rhIL-17A. Consistent with IL-6 blockade, OA-NO$_2$ inhibited rhIL-17A-induced NF-κB phosphorylation in NHDFs, compared to OA and vehicle controls (Fig. 5B). Our data suggests that the modulatory effect that OA-NO$_2$ has on fibroblasts inflammation is, in part, mediated through the limitation of NF-κB activation by inhibiting p65 phosphorylation, along with suppression of IL-6, which is important for Th17 differentiation and promotion of keratinocyte proliferation [32,42].

STAT3 is a key mediator of IL-6 functions in numerous cell types, including keratinocytes, and participates in the regulation of genes controlling survival, proliferation, and angiogenesis [27,38]. Therefore, we further assessed the effect of OA-NO$_2$ on STAT3 signaling in HaCaT cells, a human keratinocyte cell line. Following a pretreatment with OA-NO$_2$, IL-6-dependent STAT3 nuclear translocation was inhibited compared to vehicle control and OA treatment groups, as demonstrated by immunofluorescence microscopy (Fig. 5C). Consistent with these

Fig. 5. OA-NO$_2$ inhibits NF-κB and STAT3 signaling *in vitro*. (A) IL-6 transcript expression in NHDF cells was determined following 12 h of stimulation with rhIL-17A (50 ng/mL). Cells were preincubated with 3 μM OA or OA-NO$_2$ for 30 min. Values are expressed as mean ± SEM from 3 individual samples with each sample ran in triplicates, ****$p < 0.0001$. Data are one representative of two independent experiments. (B) NF-κB phosphorylation in NHDF cells was assessed by immunoblotting following stimulation with rhIL-17A. Cells were preincubated with 3 μM OA or OA-NO$_2$. Data are one representative of three independent experiments. (C) Nuclear translocation of STAT3 in HaCaT cells was examined by immunoflouresce microscopy following stimulation with rhIL-6 (50 ng/mL) for 1 h, with pretreatment of 3 μM OA or OA-NO$_2$. Scale bar = 25 μm. Representative images from three independent experiments. (D) HaCaT cell nuclear and cytosolic protein extracts were assessed for STAT3 and PCNA following 1 h rhIL-6 stimulation. Representative of two independent experiments. (E–F) Basal (E) and rhIL-6-stimulated (F) phospho-STAT3 levels in HaCaT cells. (E) For basal phospho-STAT3 levels, cells were treated with indicated doses of OA or OA-NO$_2$ for 24 h. (F) For rhIL-6-stimulated phospho-STAT3 levels, cells were preincubated with 3 μM OA or OA-NO$_2$ for 30 min and then stimulated with rhIL-6 (50 ng/mL) for 1 h. Data are one representative of three independent experiments.

findings, OA-NO$_2$ also significantly suppressed IL-6-induced STAT3 phosphorylation in NHDFs (Fig. S4A). This phenomenon was further confirmed by immunoblot analysis of keratinocyte cytoplasmic and nuclear extracts (Fig. 5D). Immunoblotting results also revealed that OA-NO$_2$ suppressed both basal (Fig. 5E) and IL-6-induced (Fig. 5F) STAT3 phosphorylation at Tyr705. Phosphorylation of STAT3 is necessary for its dimerization, nuclear translocation, and DNA binding [32]. In accordance with inhibiting STAT3 activation, OA-NO$_2$ impaired keratinocyte growth in a dose- and time-dependent manner as observed by cellular proliferation assay (Fig. S5). Moreover, OA-NO$_2$ also inhibits TNF-α-induced NF-κB phosphorylation in HaCaT cells (Fig. S4B). While prior studies applying OA-NO$_2$ topically to inflamed skin perpetuated the inflammatory response [43], here we demonstrate that OA-NO$_2$ applied directly *in vitro* to keratinocytes had an anti-inflammatory effect. This data further supports our prior findings that the inflammatory response potentiated *in vivo* by topically applied OA-NO$_2$, does not occur through keratinocyte stimulation [43]. Overall, our *in vitro* data demonstrates that OA-NO$_2$ inhibits NF-κB and STAT3 signaling and exerts anti-inflammatory as well as anti-proliferative effects on fibroblasts and keratinocytes.

2.5. Molecular mechanisms accounting for OA–NO$_2$–dependent STAT3 inhibition

The alkenyl nitro group of NO$_2$-FA provides an electrophilic character to the β-carbon of the nitroalkene, facilitating Michael addition reactions with biological nucleophiles such as protein cysteine and histidine residues. This nitroalkylation reaction is reversible and redox-dependent [44]. NO$_2$-FA display pleiotropic anti-inflammatory actions by nitroalkylating several redox-sensitive transcription factors and proteins including PPARγ, p65 (NF-κB), Keap1 (Nrf2), STING, and heat-shock factors [6,14,15,37]. Therefore, we tested whether OA-NO$_2$ inhibits STAT3 phosphorylation by direct nitroalkylation of STAT3. HaCaT cells were treated with either biotin-OA-NO$_2$ or biotin-OA, control, and cell lysates were analyzed by streptavidin-agarose pulldown assay. As demonstrated in Fig. 6A, the extent of STAT3-OA–NO$_2$–biotin adduct formation was increased in a dose-dependent manner (1.25–10 μM). Non-electrophilic biotinylated OA did not associate with STAT3. In order to further demonstrate the reversibility of this modification, cells were stimulated with biotin-OA-NO$_2$ for 2 h, followed by N-acetylcysteine (NAC) for another 2 h. NAC is a prodrug for L-cysteine and acts as a precursor of reduced glutathione (GSH). The nitroalkylated form of STAT3 was significantly suppressed by NAC treatment (Fig. 6B). Since both NAC and GSH potentially denitroalkylate target proteins [44–46], these observations support the reversibility of STAT3 nitroalkylation. In order to verify the inhibition of STAT3 phosphorylation by OA–NO$_2$–mediated nitroalkylation, we further assessed the reversibility of STAT3 phosphorylation by NAC treatment. HaCaT cells were treated with OA-NO$_2$ for 2 h, followed by increasing doses of NAC for another 2 h. Finally, cells were stimulated by IL-6 for 1 h. Consistent with previous data, OA-NO$_2$ inhibited IL-6-induced STAT3 phosphorylation. Notably, the suppressive effect of OA-NO$_2$ was reversed in a dose-dependent manner by NAC (Fig. 6C). These data indicate that OA-NO$_2$ can reversibly inhibit phosphorylation of STAT3 by direct nitroalkylation of STAT3, which is thiol redox state sensitive and more likely to occur in an oxidative environment such as psoriasiform inflammation where thiol levels are diminished. Moreover, these studies demonstrate that STAT3 nitroalkylation inhibits STAT3 Tyr705 phosphorylation. This could be through the inhibition of JAK2-dependent phosphorylation. Similarly, S-nitrosation of STAT3 at cysteine 259 has been shown to inhibit JAK2-mediated phosphorylation [47].

2.6. OA-NO$_2$ suppresses Th17 and Th1 cell differentiation

In vivo studies demonstrate that both Type 1 and Type 17 inflammatory cytokines are suppressed by OA-NO$_2$. To further assess cellular mechanisms of OA-NO$_2$, we examined the effect of OA-NO$_2$ on Th17 and Th1 differentiation in an *in vitro* setting utilizing naive CD4$^+$ T cells isolated from peripheral blood mononuclear cells. Following 5 d of Th17- or Th1-polarizing cytokine induction, production of IL-17A and IFN-γ was measured, respectively, by ELISA. As depicted in Figs. S6A and B, OA-NO$_2$ significantly suppressed IL-17A and IFN-γ production, compared to vehicle controls. Thus, OA-NO$_2$ has the capacity to directly inhibit Th17 differentiation in an effort to block psoriasiform inflammation.

Psoriasis is a chronic cutaneous inflammatory disease characterized by hyperproliferative keratinocytes, inflammatory cell infiltration, and angiogenesis. Although the etiology of psoriasis development is yet to be
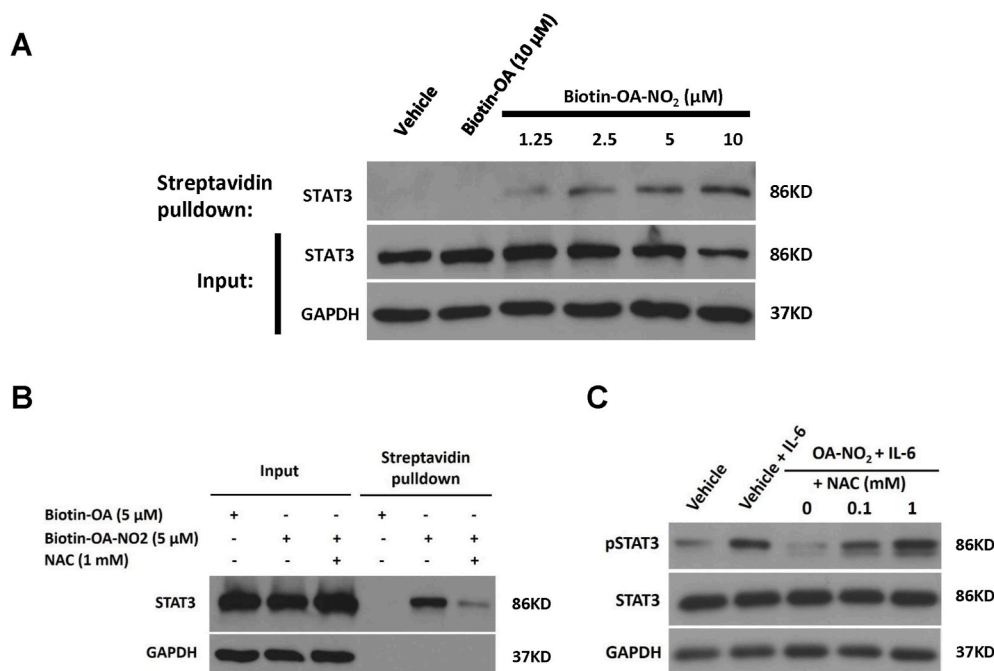
Fig. 6. OA-NO$_2$ inhibits activation of STAT3 by nitroalkylation. Nitroalkylation of STAT3 in HaCaT cells was assessed utilizing biotinylated OA-NO$_2$ and streptavidin-agarose pulldown assays. (A) HaCaT cells were treated with the indicated concentrations of biotinylated-OA or biotinylated-OA-NO$_2$ for 2 h. (B) HaCaT cells were treated with 5 μM biotinylated-OA or biotinylated-OA-NO$_2$ for 2 h then incubated with or without 1 mM NAC for another 2 h. (C) RhIL-6-stimulated phospho-STAT3 levels in HaCaT cells were determined utilizing immunoblot techniques. HaCaT cells were treated with or without OA-NO$_2$ for 2 h, followed by increasing doses of NAC for another 2 h, and then stimulated with IL-6 for 1 h. Data are one representative of three independent experiments.

fully understood, there has been substantial progress in understanding psoriasis pathogenesis in recent years. A common set of effectors, including cytokines such as IL-23 and IL-17, and transcription factors such as NF-κB and STAT3, are involved in psoriasis pathogenesis [48]. In this regard, resolution of psoriasis correlates with the inhibition of the IL-17 response [49]. Both IL-6 and STAT3 are essential modulators of Th17 differentiation and function, through a positive feedback loop that enhances expression of IL-6 and IL-17, and phosphorylation of STAT3 [38,39]. As STAT3 is a central signaling factor in Th17 differentiation, blockade of IL-17A by OA-NO$_2$ is likely dependent, in part, on the inhibition of STAT3 activation [50]. Moreover, IL-23-mediated STAT3 activation has a critical role in the upregulation of IL-17 secretion and IL-23 receptor expression, as well as Th17 maturation and survival [51–53]. In the current study, we demonstrate the capability of OA-NO$_2$ to inhibit psoriasiform dermatitis in both acute and chronic murine models. In this regard, OA-NO$_2$ suppressed the expression of critical inflammatory cytokines such as IL-1β, IL-6, and IL-17A. Mechanistically, we have determined that OA-NO$_2$ blocks the IL-17A/IL-6 positive feedback loop and suppresses cutaneous inflammation through NF-κB and STAT3 signaling blockade (Fig. S7). It is hypothesized that NF-κB and STAT3 trigger the mechanisms that induce cutaneous inflammatory diseases, including psoriasis. Thus, NF-κB and STAT3 suppression are viable therapeutic approaches to treating psoriasis [48].

3. Conclusion

In summary, our studies demonstrate that oral treatment with OA-NO$_2$ has both preventative and therapeutic effects on psoriasiform inflammation. In line with this finding, OA-NO$_2$ downregulated the production of psoriasis-dependent inflammatory cytokines in the skin, including IL-1β, IL-23, IL-6, and IL-17. *In vitro* experiments demonstrated that OA-NO$_2$ decreases both basal IL-6 levels and IL-17A-induced expression of IL-6 through the inhibition of NF-κB phosphorylation. Additional novel findings are that a) OA-NO$_2$ diminishes STAT3 phosphorylation and nuclear translocation, which inhibits keratinocyte proliferation and b) OA-NO$_2$ regulates STAT3 activation by post-translational modification of STAT3 via nitroalkylation. Overall, these results confirm the critical role of both NF-κB and STAT3 in psoriasiform dermatitis and highlight the potential of NO$_2$-FA and other small molecule nitroalkenes as therapeutic agents for the treatment of cutaneous inflammatory diseases, such as psoriasis.

4. Materials and methods

4.1. Materials

OA, OA-NO$_2$, and biotinylated OA-NO$_2$ were synthesized, purified, and quantitated as previously described [7]. Biotinylated OA was purchased from Cayman Chemical (Ann Arbor, MI). The concentration of OA-NO$_2$ was calculated gravimetrically or spectrophotometrically using the following extinction coefficients in phosphate buffer, OA-NO$_2$, λ_{268} 8.22 M^{-1}cm^{-1}. Primary antibodies for immunoblotting studies were obtained from the following sources: GAPDH (Cell Signaling Technology, Beverly, MA, catalog 5174S), β-Actin (Cell Signaling Technology, catalog 4970S), PCNA (Cell Signaling Technology, catalog 13110S), β-Tubulin (Cell Signaling Technology, catalog 86298S), NF-κB (Cell Signaling Technology, catalog 8242), p65NF-κB (Ser536) (Cell Signaling Technology, catalog 3033S), STAT3 (Cell Signaling Technology, catalog 12640S) or pSTAT3 (Tyr705) (Cell Signaling Technology, catalog 9145S). Aldara/Imiquimod was purchased from 3M Pharmaceuticals.

4.2. Cell culture

HaCaT cells were purchased from AddexBio (San Diego, CA). NHDF cells were purchased from Lifeline Cell Technology (Oceanside, CA). Both cells were maintained in high glucose DMEM with 10% FBS,

supplemented with 2 mM-glutamine, 100 U/mL penicillin, and 100 μg/mL streptomycin. HaCaTs and NHDFs were cultured in serum-free DMEM for 12 h prior to stimulation with IL-6 or IL-17A.

4.3. Animals

C57BL/6 wild type (WT) and K14-VEGF (FVB background) mice were purchased from Jackson Laboratories (Bar Harbor, ME), K5-IL-17C mice (C56BL/6 background) were a kind gift from Nicole Ward. Male and female mice were used between the ages of 6–8 weeks (C57Bl/6), 9–10 wks (K14-VEGF: therapeutic model), 6–8 wks K14-VEGF (preventative model), and 8–10 wk (K5-IL-17c model). For the transgenic models, K14-VEGF mice in the therapeutic studies had fully developed a psoriasiform dermatitis with an ear thickness of 0.5 mm or greater and the development of red scaly plaques on both ears and face. The K14-VEGF mice in the preventative studies did not have signs of inflammation and an ear thickness of less than 0.4 mm. For the therapeutic K5-IL-17c mouse studies, the mice had developed a full-fledged psoriasiform dermatitis with significant hair loss and lesional development (red scaly plaques) on the dorsal neck and back. Mice were bred and housed under specific pathogen-free conditions. All mice were treated according to the University of Pittsburgh's Institutional Animal Care Guidelines and the NIH guide for the care and use of laboratory animals.

4.4. Oral delivery and dose selection

For oral administration, 100 μL of a suspension containing 0.2 mg of OA-NO$_2$, in an emulsion made of liposomes containing soybean oil, medium-chain triglycerides, and egg lecithin was delivered via gavage. 0.2 mg/mouse was selected based on prior studies [8] and initial dose-response curves (data not shown). In this regard, an initial study was performed with oral OA-NO$_2$ in a CHS model to compare oral and subcutaneous (SC) dosing from the prior CHS studies [8], the dose range was 0.05, 0.1, 0.2, and 0.4 mg/mouse. The 0.2 mg/mouse dose was the most efficient dose for suppressing ear thickness in both the oral and SC dosing groups. These studies were repeated in the IMQ model of psoriasis using 0.05, 0.1, 0.2, and 0.4 mg/mouse dosing range and again the 0.2 mg/mouse dose was the most efficient dose to suppress ear thickness, one of our primary endpoint measurements.

4.5. IMQ-induced psoriasiform dermatitis in mice

C57BL/6 mice received a topical dose of 62.5 mg of IMQ cream (5% Aldara) or control cream (Vanicream, Pharmaceutical specialties, Rochester, MN) on the depilated back and ears for 6 consecutive days, as previously described [18]. 18 hr prior to IMQ application, OA-NO$_2$ [0.2 mg/mouse] or vehicle (an emulsion made of liposomes containing soybean oil, medium-chain triglycerides, and egg lecithin) were orally administered. Ear thickness measurements were performed daily for 120 h using electronic calipers (Mitutoyo, Aurora, IL). On day 6 mice were sacrificed and ears collected and fixed in formalin for histological assessment, or frozen and homogenized for immunoblotting or ELISA. Alternatively, mice were sacrificed on day 2 following IMQ application and ear tissues were collected for RNA extraction.

4.6. IL23-induced psoriasiform dermatitis in mice

C57BL/6 mouse ears were injected intradermally with 1 μg recombinant mouse (rm)IL-23 (eBioscience, San Diego, CA) in 20 μl phosphate-buffered saline (PBS) or vehicle control. OA-NO$_2$ (10 mg/kg) or vehicle control were orally administered 18 h prior to IL-23 injections. Injections and oral treatments were administered every other day for 10 d. Ear thickness was measured daily. Mice were sacrificed on day 10 and ear tissues collected and fixed in formalin for histological study or prepared for RNA extraction.

4.7. Real-time quantitative RT-PCR

Total RNA was extracted from tissues and cells utilizing TRI-reagent (Molecular Research Center, Cincinnati, OH), quantified utilizing a NanoDrop (DeNovix, Wilmington, DE), and reverse-transcribed using the QuantiTect Reverse Transcription Kit according to manufacturer's instructions (Qiagen, Hilden, Germany). Real-time quantitative PCR was performed utilizing Taqman Gene Expression Master Mix (Life Technologies, Carlsbad, CA) according to manufacturer's instructions. Taqman primers utilized were specific for ActB (endogenous control), IL-1β, IL-6, IL-17A, TNF-α, and IL-23. Reactions were run in triplicates and analyzed on a StepOne Plus sequence detection system (Applied Biosystems, Waltham, MA). Relative fold-changes of RNA transcript expression levels were normalized based on the $2^{-\Delta\Delta Ct}$ method.

4.8. Immunoblotting

Cells and tissues were lysed in RIPA buffer [with addition of 1 mM Na$_3$VO$_4$, 10 mM NaF, and Protease Inhibitor Cocktail (Sigma Aldrich, St Louis, MO; cocktail contains aprotinin, bestatin, E−64, leupeptin, and pepstatin A)] and protein concentration was determined by Pierce BCA Protein Assay. Equal amounts of lysate (10–30 μg) were subjected to SDS-PAGE. Immunoblotting was performed utilizing GAPDH, β-Tubulin, or β-Actin were assessed as protein loading controls and PCNA was assessed as a marker for nuclear protein. Primary antibodies (1:1000) were detected by enhanced chemiluminescence utilizing horseradish peroxidase-conjugated secondary antibodies (1:5000; Santa Cruz Biotechnology, Dallas, TX) and ECL substrate (GE Healthcare, UK Ltd).

4.9. ELISA

Cutaneous tissues were lysed using homogenizer tubes in PBS +1% NP-40 (v/v) supplemented with Protease inhibitor cocktail (Sigma Aldrich). Protein concentration was determined by Pierce BCA Protein Assay. Equal amounts of the skin homogenates (100 μg) or cell culture supernatants (100 μL) were analyzed for detection of cytokine secretion. Samples were assayed by ELISA according to the manufacturer's instructions using corresponding kits for mouse IL-6 (BD Biosciences, catalog 555240), human IFN-γ (BD Biosciences) and human IL-17A (R&D Systems, Inc., Minneapolis, MN, catalog DY317-05). All ELISA plates were analyzed using a SpectraMax 340 PC microplate reader (Molecular Devices). Samples were analyzed in triplicates.

4.10. Microscopy

Cross sections of mouse skin was prepared and stained as previously described [54]. Briefly, ear or dorsal skin was dissected and fixed with 10% phosphate buffered formalin for 24–72 h and then dehydrated and embedded in paraffin. Cross-sections (5 μm) were cut and stained with hematoxylin and eosin (H&E).

4.11. In vitro determination of NF-κB and STAT3 activation

Immunoblotting was performed with antibodies specific for GAPDH, STAT3, pSTAT3 (Tyr705), NF-κB or pNF-κB (Ser536) (Cell Signaling Technology). In immunofluorescence experiments, cells were fixed with 4% paraformaldehyde, permeabilized with 0.1% Triton X-100, and immunostained using anti-STAT3 (Cell Signaling Technology) followed by Alexa Fluor 488 secondary antibody (Invitrogen, Carlsbad, CA). In the semi-quantitative analysis of cytoplasmic-nuclear STAT3 localization, cells were processed according to the NE-PER cytoplasmic/nuclear subcellular fractionation kit (Thermo Scientific, Rockford, IL).

4.12. Nitroalkylation assay

Cells treated with Biotin-OA-NO$_2$ or Biotin-OA were washed with PBS, harvested, and lysed in RIPA buffer. Protein from total cell lysates was purified with Amicon Ultra-2 3K Centrifugal Filter Unit (Merck Millipore Darmstadt, Germany). 500 μg of total cellular proteins were incubated with Streptavidin Agarose Resin (Thermo Scientific) overnight at 4 °C. Resin was washed 4 × with RIPA buffer. Protein was eluted in an equivalent volume of 2 × Gel Sample Loading Buffer (BioRad, Hercules, CA) containing 10 mM β-mercaptoethanol at 95 °C for 3 min and analyzed by 10% SDS-PAGE and immunoblotted with STAT3-and GAPDH-specific antibodies.

4.13. Isolation of naïve T cells and differentiation of Th1 or Th17 cells in vitro

Whole blood leukopaks from healthy adult donors were purchased from the Pittsburgh Central Blood Bank, with the approval of the University of Pittsburgh Institutional Review Board. PBMCs were isolated from the buffy-coat by Ficoll-Paque Plus (GE Healthcare Bio-Science AB) density gradient centrifugation. CD4$^+$ T cells were isolated with the naïve T Cell Isolation Kit (Miltenyi Biotec Inc., Bergisch Gladbach, Germany). The isolated naïve CD4$^+$ T cells were cultured in 96-well plates at a density of 4×10^4 cells/well. For Th0 cell cultures, cells were activated with 10 μg/mL plate-bound human anti-CD3 (PeproTech, Cranbury, NJ) and 1 μg/mL soluble anti-CD28 (PeproTech, catalog 10311–20) for 5 days under nonpolarizing conditions. For Th1 or Th17 cell differentiation, cells were cultured utilizing Human Th1 or Th17 Cell Differentiation Kit (R&D Systems, Inc.) according to the manufacturer's instructions.

5. Statistics

Results from multiple different groups were compared using a one-way analysis of variance (ANOVA) followed by Tukey's multiple comparison post-hoc test. Changes to groups that occurred overtime were compared by a two-way ANOVA followed by a Bonferroni post-hoc test. Comparison of two means was performed by a 2-tailed Student's T-test. A p value < 0.05 was considered statistically significant. Each experiment was repeated 2–3 times.

Data availability

No datasets were generated or analyzed during the current study.

Author contributions

Conceptualization: ARM, PW, BAF, FJS, LKF, LDF; Data Curation: PW, MEK, TLS, ARM; Formal Analysis: PW, TLS, ARM; Funding Acquisition: ARM, LDF, FJS; Investigation: PW; Resources: ARM, LDF, BAF, FJS, LKF; Supervision: ARM, TLS; Validation: ARM, TLS; Writing-Original Draft Preparation: PW, ARM; Writing-Review and Editing: FJS, BAF, ARM, LKF, LDF, MEK, TLS.

Declaration of competing interest

BAF and FJS acknowledge financial interest in Creegh Pharma, Inc. LDF has financial interest in SkinJect and Brainstage. The other authors have declared that no further conflict of interest exists.

Institutes of Health.

Appendix A. Supplementary data

Supplementary data to this article can be found online at https://doi.org/10.1016/j.redox.2021.101987.

References

[1] Y. Liu, J.G. Krueger, A.M. Bowcock, Psoriasis: genetic associations and immune system changes, Gene Immun. 8 (2007) 1–12.

[2] L.M. Johnson-Huang, M.A. Lowes, J.G. Krueger, Putting together the psoriasis puzzle: an update on developing targeted therapies, Dis Model Mech 5 (2012) 423–433.

[3] N.E. Natsis, J.F. Merola, J.M. Weinberg, J.J. Wu, A.M. Orbai, J. Bagel, A. B. Gottlieb, Treatment of medicare patients with moderate-to-severe psoriasis who cannot afford biologics or apremilast, Am. J. Clin. Dermatol. 21 (2020) 109–117.

[4] K. Martina, F. Jorga, C. Petra, D. Tomas, L. Iva, A. Petr, G. Spyridon, Demographic data, comorbidities, quality of life, and survival probability of biologic therapy associated with sex-specific differences in psoriasis in the Czech Republic, Dermatol. Ther. (2021), e14849.

[5] S.B. Kaushik, M.G. Lebwohl, Review of safety and efficacy of approved systemic psoriasis therapies, Int. J. Dermatol. 58 (2019) 649–658.

[6] T. Cui, F.J. Schopfer, J. Zhang, K. Chen, T. Ichikawa, P.R. Baker, C. Batthyany, B. K. Chacko, X. Feng, R.P. Patel, A. Agarwal, B.A. Freeman, Y.E. Chen, Nitrated fatty acids: endogenous anti-inflammatory signaling mediators, J. Biol. Chem. 281 (2006) 35686–35698.

[7] L. Villacorta, Z. Gao, F.J. Schopfer, B.A. Freeman, Y.E. Chen, Nitro-fatty acids in cardiovascular regulation and diseases: characteristics and molecular mechanisms, Front. Biosci. 21 (2016) 873–889.

[8] A.R. Mathers, C.D. Carey, M.E. Killeen, J.A. Diaz-Perez, S.R. Salvatore, F. J. Schopfer, B.A. Freeman, L.D. Falo, Electrophilic nitro-fatty acids suppress allergic contact dermatitis in mice, Allergy 72 (2017) 656–664.

[9] C.M. Arbeeny, H. Ling, M.M. Smith, S. O'Brien, S. Wawersik, S.R. Ledbetter, A. McAlexander, F.J. Schopfer, R.N. Willette, D.K. Jorkasky, CXA-10, a nitrated fatty acid, is renoprotective in deoxycorticosterone acetate-salt nephropathy, J. Pharmacol. Exp. Therapeut. 369 (2019) 503–510.

[10] H. Liu, Z. Jia, S. Soodvilai, G. Guan, M.H. Wang, Z. Dong, J.D. Symons, T. Yang, Nitro-oleic acid protects the mouse kidney from ischemia and reperfusion injury, Am. J. Physiol. Ren. Physiol. 295 (2008) F942–F949.

[11] J. Zhang, L. Villacorta, L. Chang, Z. Fan, M. Hamblin, T. Zhu, C.S. Chen, M.P. Cole, F.J. Schopfer, C.X. Deng, M.T. Garcia-Barrio, Y.H. Feng, B.A. Freeman, Y.E. Chen, Nitro-oleic acid inhibits angiotensin II-induced hypertension, Circ. Res. 107 (2010) 540–548.

[12] T.K. Rudolph, V. Rudolph, M.M. Edreira, M.P. Cole, G. Bonacci, F.J. Schopfer, S. R. Woodcock, A. Franek, M. Pekarova, N.K. Khoo, A.H. Hasty, S. Baldus, B. A. Freeman, Nitro-fatty acids reduce atherosclerosis in apolipoprotein E-deficient mice, Arterioscl. Throm. Vas. 30 (2010) 938–945.

[13] L. Turell, D.A. Vitturi, E.L. Coitino, L. Lebrato, M.N. Moller, C. Sagasti, S. R. Salvatore, S.R. Woodcock, B. Alvarez, F.J. Schopfer, The chemical basis of thiol addition to nitro-conjugated linoleic acid, a protective cell-signaling lipid, J. Biol. Chem. 292 (2017) 1145–1159.

[14] E. Kansanen, G. Bonacci, F.J. Schopfer, S.M. Kuosmanen, K.I. Tong, H. Leinonen, S. R. Woodcock, M. Yamamoto, C. Carlberg, S. Ylä-Herttuala, B.A. Freeman, A.-L. Levonen, Electrophilic nitro-fatty acids activate NRF2 by a KEAP1 cysteine 151-independent mechanism, J. Biol. Chem. 286 (2011) 14019–14027.

[15] F.J. Schopfer, C. Cipollina, B.A. Freeman, Formation and signaling actions of electrophilic lipids, Chem. Rev. 111 (2011) 5997–6021.

[16] M. Fazzari, D.A. Vitturi, S.R. Woodcock, S.R. Salvatore, B.A. Freeman, F. J. Schopfer, Electrophilic fatty acid nitroalkenes are systemically transported and distributed upon esterification to complex lipids, J. Lipid Res. 60 (2019) 388–399.

[17] J. Sun, Y. Zhao, J. Hu, Curcumin inhibits imiquimod-induced psoriasis-like inflammation by inhibiting IL-1beta and IL-6 production in mice, PloS One 8 (2013), e67078.

[18] L. van der Fits, S. Mourits, J.S.A. Voerman, M. Kant, L. Boon, J.D. Laman, F. Cornelissen, A.-M. Mus, E. Florencia, E.P. Prens, E. Lubberts, Imiquimod-induced psoriasis-like skin inflammation in mice is mediated via the IL-23/IL-17 Axis, J. Immunol. 182 (2009) 5836–5845.

[19] W.R. Swindell, K.A. Michaels, A.J. Sutter, D. Diaconu, Y. Fritz, X. Xing, M. K. Sarkar, Y. Liang, A. Tsoi, J.E. Gudjonsson, N.L. Ward, Imiquimod has strain-dependent effects in mice and does not uniquely model human psoriasis, Genome Med. 9 (2017) 24.

[20] H.L. Rizzo, S. Kagami, K.G. Phillips, S.E. Kurtz, S.L. Jacques, A. Blauvelt, IL-23-mediated psoriasis-like epidermal hyperplasia is dependent on IL-17A, J. Immunol. 186 (2011) 1495–1502.

[21] M. Bhushan, B. McLaughlin, J.B. Weiss, C.E.M. Griffiths, Levels of endothelial cell stimulating angiogenesis factor and vascular endothelial growth factor are elevated in psoriasis, Br. J. Dermatol. 141 (1999) 1054–1060.

[22] M. Detmar, L.F. Brown, K.P. Claffey, K.T. Yeo, O. Kocher, R.W. Jackman, B. Berse, H.F. Dvorak, Overexpression of vascular permeability factor/vascular endothelial growth factor and its receptors in psoriasis, J. Exp. Med. 180 (1994) 1141–1146.

[23] Y.P. Xia, B. Li, D. Hylton, M. Detmar, G.D. Yancopoulos, J.S. Rudge, Transgenic delivery of VEGF to mouse skin leads to an inflammatory condition resembling human psoriasis, Blood 102 (2003) 161–168.

[24] A. Johnston, Y. Fritz, S.M. Dawes, D. Diaconu, P.M. Al-Attar, A.M. Guzman, C. S. Chen, W. Fu, J.E. Gudjonsson, T.S. McCormick, N.L. Ward, Keratinocyte overexpression of IL-17C promotes psoriasiform skin inflammation, J. Immunol. 190 (2013) 2252–2262.

[25] E. Calautti, L. Avalle, V. Poli, Psoriasis: a STAT3-centric view, Int. J. Mol. Sci. 19 (2018).

[26] P.C. Heinrich, I. Behrmann, G. Muller-Newen, F. Schaper, L. Graeve, Interleukin-6-type cytokine signalling through the gp130/Jak/STAT pathway, Biochem. J. 334 (Pt 2) (1998) 297–314.

[27] B.B. Aggarwal, A.B. Kunnumakkara, K.B. Harikumar, S.R. Gupta, S.T. Tharakan, C. Koca, S. Dey, B. Sung, Signal transducer and activator of transcription-3, inflammation, and cancer: how intimate is the relationship? Ann NY Acad Sci 1171 (2009) 59–76.

[28] R.M. Grossman, J. Krueger, D. Yourish, A. Granelli-Piperno, D.P. Murphy, L. T. May, T.S. Kupper, P.B. Sehgal, A.B. Gottlieb, Interleukin 6 is expressed in high levels in psoriatic skin and stimulates proliferation of cultured human keratinocytes, Proc. Natl. Acad. Sci. U. S. A. 86 (1989) 6367–6371.

[29] S.M. Sa, P.A. Valdez, J. Wu, K. Jung, F. Zhong, L. Hall, I. Kasman, J. Winer, Z. Modrusan, D.M. Danilenko, W. Ouyang, The effects of IL-20 subfamily cytokines on reconstituted human epidermis suggest potential roles in cutaneous innate defense and pathogenic adaptive immunity in psoriasis, J. Immunol. 178 (2007) 2229–2240.

[30] S. Sano, K.S. Chan, S. Carbajal, J. Clifford, M. Peavey, K. Kiguchi, S. Itami, B. J. Nickoloff, J. DiGiovanni, Stat3 links activated keratinocytes and immunocytes required for development of psoriasis in a novel transgenic mouse model, Nat. Med. 11 (2005) 43–49.

[31] K. Miyoshi, K. Takaishi, K. Nakajima, M. Ikeda, T. Kanda, T. Iiyama, N. Asao, J. DiGiovanni, S. Sano, Stat3 as a therapeutic target for the treatment of psoriasis: a clinical feasibility study with STA-21, a Stat3 inhibitor, J. Invest. Dermatol. 131 (2011) 108–117.

[32] J. Louten, K. Boniface, R. de Waal Malefyt, Development and function of TH17 cells in health and disease, J. Allergy Clin. Immunol. 123 (2009) 1004–1011.

[33] J.Y. Kim, J. Ahn, J. Kim, M. Choi, H. Jeon, K. Choe, D.Y. Lee, P. Kim, S. Jon, Nanoparticle-assisted transcutaneous delivery of a signal transducer and activator of transcription 3-inhibiting peptide ameliorates psoriasis-like skin inflammation, ACS Nano 12 (2018) 6904–6916.

[34] L. Tang, S. He, X. Wang, H. Liu, Y. Zhu, B. Feng, Z. Su, W. Zhu, B. Liu, F. Xu, C. Li, J. Zhao, X. Zheng, C. Lu, G. Zheng, Cryptotanshinone reduces psoriatic epidermal hyperplasia via inhibiting the activation of STAT3, Exp. Dermatol. 27 (2018) 268–275.

[35] G. Ambrozova, H. Martiskova, A. Koudelka, T. Ravekes, T.K. Rudolph, A. Klinke, V. Rudolph, B.A. Freeman, S.R. Woodcock, L. Kubala, M. Pekarova, Nitro-oleic acid modulates classical and regulatory activation of macrophages and their involvement in pro-fibrotic responses, Free Radic. Biol. Med. 90 (2016) 252–260.

[36] N.K.H. Khoo, L. Li, S.R. Salvatore, F.J. Schopfer, B.A. Freeman, Electrophilic fatty acid nitroalkenes regulate Nrf2 and NF-kappaB signaling:A medicinal chemistry investigation of structure-function relationships, Sci. Rep. 8 (2018) 2295.

[37] A.L. Hansen, G.J. Buchan, M. Ruhl, K. Mukai, S.R. Salvatore, E. Ogawa, S. D. Andersen, M.B. Iversen, A.L. Thielke, C. Gunderstofte, M. Motwani, C.T. Moller, A.S. Jakobsen, K.A. Fitzgerald, J. Roos, R. Lin, T.J. Maier, R. Goldbach-Mansky, C. A. Miner, W. Qian, J.J. Miner, R.E. Rigby, J. Rehwinkel, M.R. Jakobsen, H. Arai, T. Taguchi, F.J. Schopfer, D. Olagnier, C.K. Holm, Nitro-fatty acids are formed in response to virus infection and are potent inhibitors of STING palmitoylation and signaling, Proc. Natl. Acad. Sci. U. S. A. 115 (2018) E7768–E7775.

[38] A. Camporeale, V. Poli, IL-6, IL-17 and STAT3: a holy trinity in auto-immunity? Front. Biosci. 17 (2012) 2306–2326.

[39] H. Ogura, M. Murakami, Y. Okuyama, M. Tsuruoka, C. Kitabayashi, M. Kanamoto, M. Nishihara, Y. Iwakura, T. Hirano, Interleukin-17 promotes autoimmunity by triggering a positive-feedback loop via interleukin-6 induction, Immunity 29 (2008) 628–636.

[40] L. Villacorta, L. Chang, S.R. Salvatore, T. Ichikawa, J. Zhang, D. Petrovic-Djergovic, L. Jia, H. Carlsen, F.J. Schopfer, B.A. Freeman, Y.E. Chen, Electrophilic nitro-fatty acids inhibit vascular inflammation by disrupting LPS-dependent TLR4 signalling in lipid rafts, Cardiovasc. Res. 98 (2013) 116–124.

[41] C.C. Woodcock, Y. Huang, S.R. Woodcock, S.R. Salvatore, B. Singh, F. Golin-Bisello, N.E. Davidson, C.A. Neumann, B.A. Freeman, S.G. Wendell, Nitro-fatty acid inhibition of triple-negative breast cancer cell viability, migration, invasion, and tumor growth, J. Biol. Chem. 293 (2018) 1120–1137.

[42] M. Hernandez-Quintero, W. Kuri-Harcuch, A. Gonzalez Robles, F. Castro-Munozledo, Interleukin-6 promotes human epidermal keratinocyte proliferation and keratin cytoskeleton reorganization in culture, Cell Tissue Res. 325 (2006) 77–90.

[43] A.R. Mathers, C.D. Carey, M.E. Killeen, S.R. Salvatore, L.K. Ferris, B.A. Freeman, F. J. Schopfer, L.D. Falo, Topical electrophilic nitro-fatty acids potentiate cutaneous inflammation, Free Radic. Biol. Med. 115 (2018) 31–42.

[44] C. Batthyany, F.J. Schopfer, P.R.S. Baker, R. Durán, L.M.S. Baker, Y. Huang, C. Cerveñansky, B.P. Branchaud, B.A. Freeman, Reversible post-translational modification of proteins by nitrated fatty acids in vivo, J. Biol. Chem. 281 (2006) 20450–20463.

[45] L.M. Baker, P.R. Baker, F. Golin-Bisello, F.J. Schopfer, M. Fink, S.R. Woodcock, B. P. Branchaud, R. Radi, B.A. Freeman, Nitro-fatty acid reaction with glutathione and cysteine. Kinetic analysis of thiol alkylation by a Michael addition reaction, J. Biol. Chem. 282 (2007) 31085–31093.

[46] A.C. Geisler, T.K. Rudolph, Nitroalkylation–a redox sensitive signaling pathway, Biochim. Biophys. Acta 1820 (2012) 777–784.

[47] J. Kim, J.S. Won, A.K. Singh, A.K. Sharma, I. Singh, STAT3 regulation by S-nitrosylation: implication for inflammatory disease, Antioxidants Redox Signal. 20 (2014) 2514–2527.

[48] G.K. Perera, P. Di Meglio, F.O. Nestle, Psoriasis, Annu. Rev. Pathol. 7 (2012) 385–422.

[49] N.C. Brembilla, L. Senra, W.H. Boehncke, The IL-17 family of cytokines in psoriasis: IL-17A and beyond, Front. Immunol. 9 (2018) 1682.

[50] A. Di Cesare, P. Di Meglio, F.O. Nestle, The IL-23/Th17 axis in the immunopathogenesis of psoriasis, J. Invest. Dermatol. 129 (2009) 1339–1350.

[51] S.L. Gaffen, R. Jain, A.V. Garg, D.J. Cua, The IL-23-IL-17 immune axis: from mechanisms to therapeutic testing, Nat. Rev. Immunol. 14 (2014) 585–600.

[52] X.O. Yang, A.D. Panopoulos, R. Nurieva, S.H. Chang, D. Wang, S.S. Watowich, C. Dong, STAT3 regulates cytokine-mediated generation of inflammatory helper T cells, J. Biol. Chem. 282 (2007) 9358–9363.

[53] J.S. Samuels, L. Holland, M. Lopez, K. Meyers, W.G. Cumbie, A. McClain, A. Ignatowicz, D. Nelson, R. Shashidharamurthy, Prostaglandin E2 and IL-23 interconnects STAT3 and RoRgamma pathways to initiate Th17 CD4(+) T-cell development during rheumatoid arthritis, Inflamm. Res. 67 (2018) 589–596.

[54] A.R. Mathers, B.M. Janelsins, J.P. Rubin, O.A. Tkacheva, W.J. Shufesky, S. C. Watkins, A.E. Morelli, A.T. Larregina, Differential capability of human cutaneous dendritic cell subsets to initiate Th17 responses, J. Immunol. 182 (2009) 921–933.